A Molecular Dynamics Simulation Study on Melting of Pd-Pt Nanoclusters

Subramanian KRSS, Venkat R. Bhethanabotla[*] and Babu Joseph
Sensors Research Laboratory, Chemical Engineering Department,
University of South Florida, Tampa, Florida, 33620, USA

Abstract

Bimetallic nanoclusters are of interest because of their utility in catalysis and sensors. The thermal characteristics of bimetallic Pt-Pd nanoclusters of different sizes and compositions were investigated through molecular dynamics simulations using the Quantum Sutton-Chen (QSC) many-body potentials. Monte-Carlo simulations employing the bond order simulation model were used to generate minimum energy configurations, which were utilized as the starting point for molecular dynamics simulations. The calculated initial configurations of Pt-Pd system consisted of surface segregated Pd atoms and a Pt rich core. Melting characteristics were studied by following the changes in potential energy and heat capacity as functions of temperature. Structural changes accompanying the thermal evolution were studied by the bond order parameter method (BOP). The Pt-Pd clusters exhibited a two-stage melting: surface melting of the external Pd atoms followed by homogeneous melting of the Pt core. These transitions were found to depend on the composition and size of the nanocluster. Melting temperatures of the nanoclusters were found to be much lower than those of bulk Pt and Pd. Bulk melting of Pd and Pt simulated using periodic boundary conditions compare well with experimental values, thus providing justification for the use of QSC potentials in these simulations. Deformation parameters were calculated to characterize the structural evolution resulting from diffusion of Pd and Pt atoms. The results indicate that in Pd-Pt clusters, Pd atoms prefer to remain at the surface even after melting. In addition, Pt also tends to diffuse to the surface after melting due to reduction of its surface energy with temperature. This mixing pattern is different from those reported in some of the earlier studies on melting of bimetallics.

1. Introduction

Metal nanoparticles exhibit physical, chemical, and electronic properties different from those of bulk atoms and single molecules due to the large fraction of surface atoms. The large number of surface atoms, which depend on the size, shape, and composition of nanoparticles, leads to unique properties which make these nanoparticles suitable for applications in heterogeneous catalysis, sensors, as well as microelectronic devices. In catalysis and sensing applications, nanoclusters provide improved selectivity and sensitivity due to the high surface area offered. One such example is the palladium nanostructure, which finds use in hydrogen sensing, along with its alloys (Favier et al; Chaudhari thesis). Literature suggests that bimetallic nanoclusters of palladium exhibit superior activity, selectivity, stability, and resistance to poisoning when compared to their single metal counterparts (Sinfelt, 1983). Since the key to all applications of nanoclusters is their small size and structure, knowledge and control of their size and shape distribution, surface composition, and crystal structure is critical to improved designs of the same.

[*] Electronic address: venkat@eng.usf.edu

Considerable experimental and theoretical research has been dedicated to understanding the thermodynamics and kinetics of nanoparticle growth and stabilization when subjected to thermal and other stresses (Wang; 1998; Kusche, 1999; Schmidt, 1997; Petroski, 1998). Melting properties of the metal nanoclusters and their associated effect on shape and composition would have a bearing on the method of synthesis, processing and the performance of these nanoclusters in various areas of application. It is a well known fact that the melting points of nanoclusters decrease with decreasing cluster sizes and their values are much below the bulk melting temperatures (Cleveland, 1998; Calvo, 2000; Lei, 2001). This lowering effect is mainly attributed to the large percentage of weakly bound surface atoms which are less constrained in their thermal motions. However, there is very little quantitative data on the structure and energetics of bulk and surface regions governing the properties of such systems, and a comprehensive understanding of the same is needed. Computer simulations offer an effective tool to study properties of nanoclusters and complement ongoing experimental (Walter, 1999).

A molecular dynamics simulation study of melting, freezing, and coalescence of gold nanoclusters, in the size range of 135-3995 atoms, indicated that melting begins at the surface and proceeds inwards toward the core (Lewis, 1997). Several structural transformations are found to be precursors to cluster melting (Cleveland, 1998). MD studies on melting of Ni nanoclusters up to 8007 atoms indicated a transition from molecular behavior below 500 atoms to a mesoscale regime above 750 atoms with well defined bulk and surface properties (Qi, 2001). The final atomic arrangements in Au nanoclusters have been found to be strongly influenced by thermodynamic factors and growth kinetics (Chaushak, 2001), which is likely the case for transition metals and alloys. Potential energy distribution of transition metal clusters showed the coexistence of a surface-melted phase with solid core for clusters larger than 200 atoms (Lee, 2001). The phase change was mainly attributed to isomerization transitions, as no pre-melting peak was detected in the heat capacity curves. A non-monotonic variation of melting temperature with cluster size is found for very small sized clusters (Calvo, 2000). Experimental studies on tin nanoclusters having 10-30 atoms corroborate this finding (Shvartsburg, 2000).

While single component metal clusters have been extensively investigated, much less attention has been devoted to the study of bimetallic nanoclusters. In addition to the inter-atomic interactions, the properties of bimetallics are influenced by relative concentrations. Additional complexity in these systems results from the surface segregation phenomenon and micro-mixing at the surface. Earlier work on MD simulations of bimetallic Cu-Ni nanocluster indicated a two staged melting process in which surface melting of Cu was followed by homogeneous melting of the Ni core (Huang, 2002). A Cu-Au cluster does not experience a smooth transition from a pure Cu like behavior to a pure Au cluster with a decrease in the concentration of Cu (Lopez, 1996). Also, the thermal behavior of Cu-Au is mainly influenced by presence of Cu atoms in the bimetallic. Cluster melting of Al coated Pb suggested dependence of the two-stage melting process on the relative orientation of crystal core to that of coating (Jin, 1999). MD studies on melting and freezing of Ni-Al clusters of various compositions indicated surface segregated Al to inhibit nucleation in Al-rich and equi-atomic bimetallic clusters leading to formation of amorphous aggregates (Chausak, 2003). However, in all previous studies, the size and composition effects on the melting behavior of bimetallic nanoclusters have not been addressed. In the present paper, we explore the melting behavior

of Pd-Pt clusters of different compositions ranging from Pd rich system to a cluster rich in Pt employing MD simulations using the Quantum Sutton Chen (QSC) potential (Qi, 1999).

2. Initial Configuration Set-up

Both palladium and platinum are metals having an FCC structure. An FCC block was first constructed from an FCC unit cell by replication in the ABC direction with centre located at (0, 0, 0). Nanoclusters were constructed from this large FCC block of Pd-Pt, using various spherical cut-off radii, leading to a smooth but facetted surface structures.

The cluster cut off radius is defined as

$$R_c = R_g \sqrt{\frac{5}{3}} + R_i \tag{2.1}$$

where the inter atomic radius for the Pd-Pt system, R_i =1.37 A and radius of gyration R_g is given by,

$$R_g^2 = \frac{1}{N} \sum_j (R_j - R_{cm})^2 \tag{2.2}$$

where, $(R_j - R_{cm})$ is the distance of atom j from the cluster center of mass.

The generated structure was then subjected to a Metropolis Monte-Carlo simulation employing a bond order simulation (BOS) model (Zhu, 1997), to generate the minimum energy initial configuration, used subsequently for studying the melting phenomena. The parameters used in the BOS model are listed in Table 1. Molecular and mesoscale regimes are observed for Ni nanoclusters with atoms less than 500 and greater than 750, respectively (Qi, 2001). Hence, we consider clusters ranging from 456 atoms to 1088 atoms to take into account a variety of size ranges in both the molecular and mesoscale region.

Table 1. Parameters for BOS model used in MC simulations (Yang, 1994)

Component	ε_1 (eV)	ε_9 (eV)	ε_{12} (eV)	ΔE_{12} (eV)	λ(eV)
Pd	-0.52	-2.999	-3.89	-0.08751	0
Pt	-1.55	-4.8	-5.84	0.0751	0

3. Computational Details for the Melting Study

3.1 Potential Function

MD simulations using DLPOLY were used to gain insights into the melting process at the atomistic level. The Sutton-Chen potential been used to predict the thermodynamic properties of transition metal clusters. Based on the Sutton-Chen potential, the potential energy of the finite system is given by,

$$U_{tot} = \sum_i U_i = \sum_i \varepsilon \left[\sum_{j \neq i} \frac{1}{2} V(r_{ij}) - c\rho_i^{1/2} \right] \quad (3.1)$$

Here, V (r_{ij}) is a pair potential to account for the repulsion resulting from Pauli's exclusion principle.

$$V(r_{ij}) = \left(\frac{a}{r_{ij}} \right)^n \quad (3.2)$$

The local density accounting for cohesion associated with any i^{th} atom is given by,

$$\rho_i = \sum_{j \neq i} \phi(r_{ij}) = \sum_{j \neq i} \left(\frac{a}{r_{ij}} \right)^m \quad (3.3)$$

Sutton and Chen restricted values of m to be greater than 6 and fitted it to give close agreements with bulk modulus and the elastic constants. Our studies on Pd-Pt system, using Sutton-Chen potential, indicated an appreciable movement of atoms even at 300K for Pd-Pt system, which is physically unlikely. A modification of the Sutton-Chen potential, Quantum Sutton-Chen (QSC) (Cagin, 1999; Qi, 1999, 2001, 2002) which includes quantum corrections gave better temperature behavior for the Pd-Pt bimetallic. Bulk properties of Pd and Pt predicted using QSC potential were in good agreement with experiment. Therefore we have used QSC potential function in all our nanocluster studies presented here.

Both the Sutton-Chen and the QSC parameters for the Pd and Pt are listed in Table 2. The geometric mean was used to obtain the energy parameter ε and the arithmetic mean was used for the remaining parameters, to predict the nature of interaction between Pd and Pt.

Table 2. Potential parameters used in MD simulations for Pd-Pt clusters

Sutton-Chen	n	m	ε (eV)	C	a(A)
QSC (Pd)	12	6	3.2864e-3	148.205	3.8813
SC(Pd)	12	7	4.126e-3	108.526	3.2900
QSC(Pt)	11	7	9.7894e-3	71.336	3.9163
SC(Pt)	10	8	1.9768e-3	34.428	3.9200

3.2 MD simulation Details

The MD simulations were carried out in an ensemble approximating the canonical with a constant number of atoms N and volume V (much larger than the cluster size) without any periodic boundary conditions. A constant temperature Berendson thermostat with a relaxation time of 0.4 ps was used. The equations of motion were integrated using the Verlet-leapfrog algorithm. The spherical cluster was initially subjected to mild annealing in the 0-300 K interval. This was followed by heating to 1800 K in increments of 100 K. Near the melting point, the temperature increments were reduced to 10 K to account for the large temperature fluctuations.

4. Results and Discussion

4.1 Melting Point Identification

The transition temperature from solid to liquid phase is usually identified by studying the variation in either the thermodynamic properties such as potential energy and specific heat capacity or some structural properties such as Bond Order Parameter and Wigner values. The present study employs both these methods to identify melting points for different cluster sizes and compositions. The details are discussed in subsequent sections.

4.1.1 Thermodynamic Properties

Figure 1 (a) shows the temperature dependence of potential energy for a $(Pd_{0.5}$-$Pt_{0.5})_{456}$ atom cluster. The transition from a solid to a liquid phase can be identified by a simple jump in the total potential energy curve. This corresponds to a melting temperature of 1290 ±10K for $(Pd_{0.5}$-$Pt_{0.5})_{456}$ as seen in Figure 1 (a) and 1460 ±10K for $(Pd_{0.5}$-$Pt_{0.5})_{1088.}$ The same is corroborated by calculating specific heat capacity as a function of fluctuations in the potential energy $< (\delta E_p)^2 >$ (Morishita, 2000) as given in Eqn. (4.1).

$$C_v = \frac{k < (\delta E_p)^2 >}{(kT)^2 - 2\alpha < (\delta E_p)^2 > / 3N} \tag{4.1}$$

where $< (\delta E_p)^2 > = < E_p^2 > - < E_p >^2$ and α is the ratio of the standard deviations of kinetic and potential energies.

$$\alpha = \sqrt{< (\delta KE)^2 > / < (\delta Ep)^2 >} \tag{4.2}$$

The maximum in the specific heat capacity corresponds to the temperature where a jump in potential energy is observed for both $(Pd_{0.5}$-$Pt_{0.5})_{456}$ and $(Pd_{0.5}$-$Pt_{0.5})_{1088.}$ Melting point for clusters with different compositions is discussed in subsequent sections.

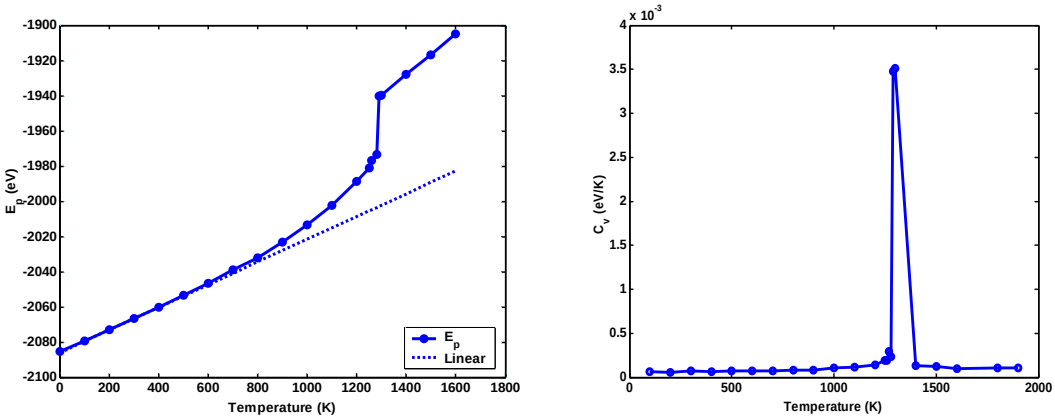

(a) **(b)**

Figure 1. Variation of thermodynamic properties with temperature for the $(Pd_{0.5}\text{-}Pt_{0.5})_{456}$ cluster (a) potential energy (b) specific heat capacity at constant volume

4.1.2 Bond Order Parameter

Bond Order Parameter method (Steinhardt, 1983) is one of the several criteria's used to analyze cluster structure as well as to distinguish between atoms in solid (closed pack) and liquid environment generated at the onset of melting. The value of the global bond order parameter Q_l in a solid cluster depends on the relative bond orientations and has a unique value for each crystal structure as reported in Table 3.

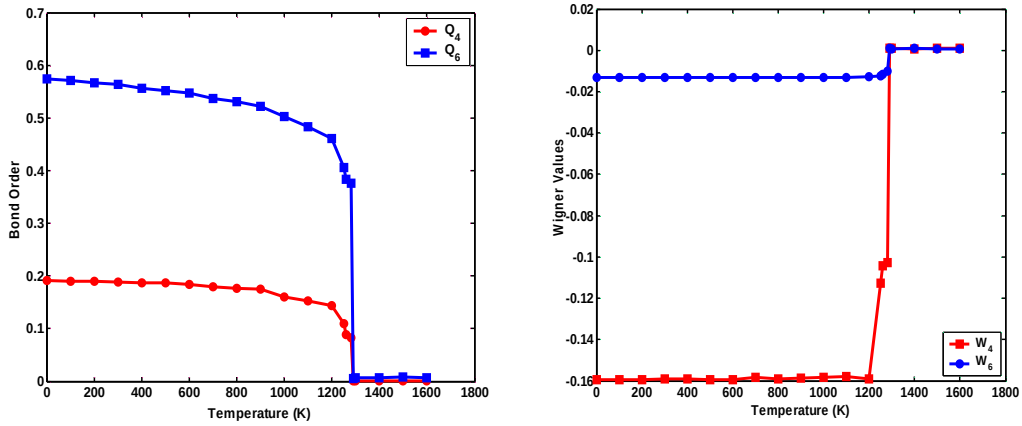

(a) **(b)**

Figure 2. Temperature dependence of the (a) global order parameter Q_4 (circles) and Q_6 (squares) cluster and (b) the global Wigner values W_4 (circles) and W_6 (squares) for $(Pd_{0.5}\text{-}Pt_{0.5})_{456}$

Table 3. Bond Order Parameter and Wigner values for various geometries

Geometry	Q_4	Q_6	W_4	W_6
FCC	0.19094	0.57452	-0.159317	-0.013161
HCP	0.09722	0.48476	0.134097	-0.012442
BCC	0.03637	0.51069	0.159317	0.013161
Icosahedral	0	0.66332	0	-0.169754
Sc	0.76376	0.35355	0.159317	0.013161
Liquid	0	0	0	0

The Q_6 and W_6 values show transition from a FCC based cluster to a somewhat HCP symmetry near the melting point in the temperature range 1200-1290 K for both $(Pd_{0.5}\text{-}Pt_{0.5})_{456}$ and $(Pd_{0.5}\text{-}Pt_{0.5})_{1088}$ clusters. The melting point can be estimated from the variation in the bond order parameter values as shown in Figure 2.

At the melting point, all the order parameters and Wigner values (Figure 2) change rapidly to zero indicating a transition to isotropic liquid phase. Similar behavior is observed for the $(Pd_{0.5}\text{-}Pt_{0.5})_{1088}$ cluster. We find the melting point to be 1290 ± 10 K and 1460 ± 10 K for $(Pd_{0.5}\text{-}Pt_{0.5})_{456}$ and $(Pd_{0.5}\text{-}Pt_{0.5})_{1088}$ which is consistent with those obtained from the thermodynamic properties.

4.2 Understanding the Melting Phenomenon

4.2.1 Analysis of Density Profiles

To understand the melting characteristics of the bimetallics, we analyzed the radial density profile of Pd and Pt, as shown in Figure 3. The surface segregation of Pd atoms is clearly visible from the initial density profile of Pd and Pt at 300 K (Figure 3 (a)). As the temperature increases (900 K -1100 K), we find that the outer most peaks in the radial density profile of Pd merge and become broader suggesting surface melting (Figure 3 (b)). However, the inner core consisting mostly of Pt is still crystalline which is evident from the well defined inner peaks in the Pt radial density profile Figure 3 (c). But above 1290 K we find liquid like behavior for Pt atoms which corresponds to the homogeneous melting temperature predicted for $(Pd_{0.5}\text{-}Pt_{0.5})_{456}$ (Figure 3 (b) and (c)).

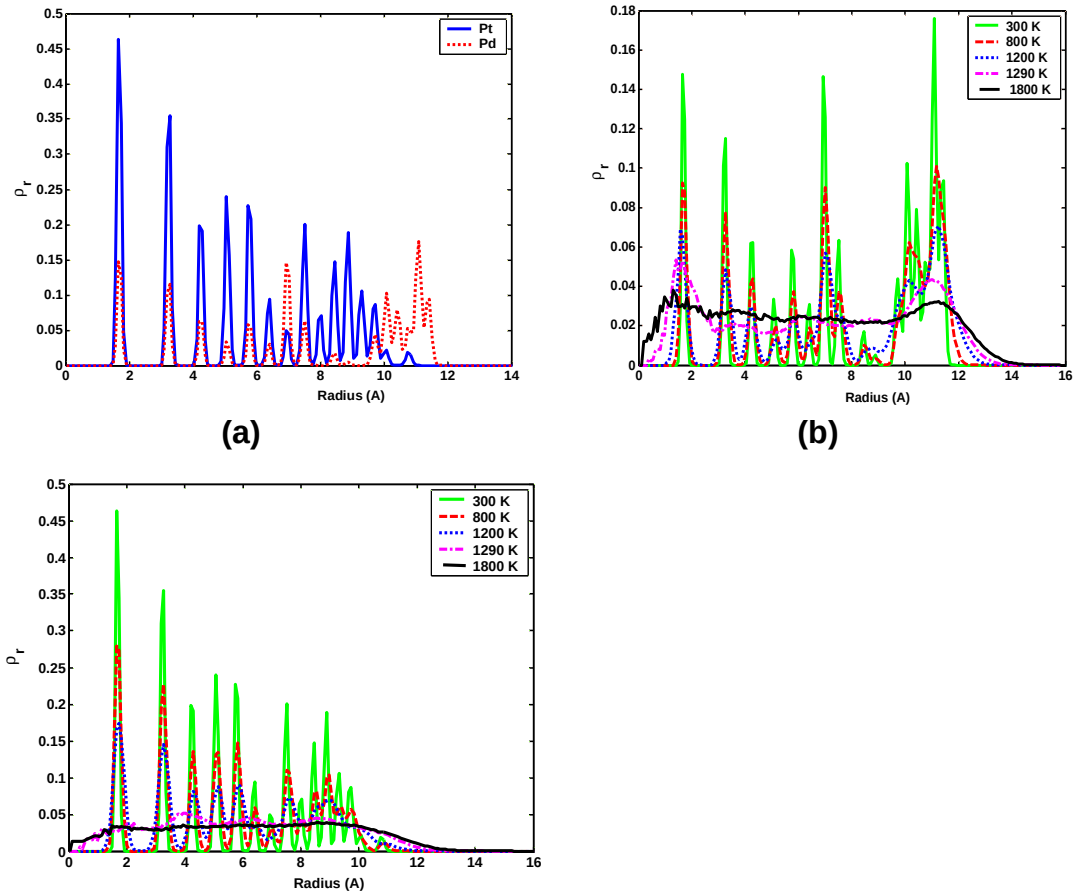

Figure 3. Radial density profile for $(Pd_{0.5}\text{-}Pt_{0.5})_{456}$ cluster. (a) Initial atomic distribution after annealing at 300 K. (b) Atomic distribution of Pd in radial direction before and after melting transition. (c) Atomic distribution of Pt in radial direction showing melting transition

4.2.2 Deformation Parameters:

Transformations resulting due to diffusion of Pd and Pt atoms during the melting process can be characterized using deformation parameters (Huang and Balbuena, 2002) given by,

$$\varepsilon_q = \frac{\sum_{i=1}^{N} | q_i - q_{cen} |}{N} \tag{4.3}$$

where q_i refers to either the position coordinates of i^{th} atom in an N atom cluster along one of the three (x, y, z) directions, or the position vector **r**(x, y, z) and q_{cen} is the cluster center of mass.

The initial nanocluster shape is spherical at 300K. The radial deformation parameters of Pt are lower than that of Pd indicating a preferential location of Pt at the cluster core. Figure 4 indicates that ε_r increases with temperature indicating an outward diffusion of both Pd and Pt up to 1100 K. However, near the melting point there is a sharp change in deformation parameters of both Pd and Pt. The overall deformation parameter increases rapidly because of the net outward diffusion of Pt atoms.

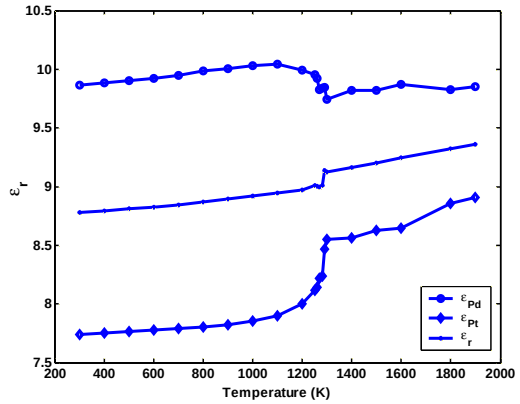

Figure 4. Variation of radial deformation parameters with temperature for $(Pd_{0.5}\text{-}Pt_{0.5})_{456}$

ε_r^{Pt} shows a slight increase initially between 300 K and 1100 K. Between 1100 K and 1200 K, ε_r^{Pt} shows slightly larger changes, followed by a rapid one near the melting point and continues to increase in the liquid phase. This indicates the tendency of the Pt atoms to move to the surface with increasing temperature. However, the decrease in ε_r^{Pd} is not the same as the increase in ε_r^{Pt}. The overall cluster shape has to change to accommodate the increased number of surface atoms. The shape of the cluster now changes from a spherical to a somewhat oval shape. This behavior is somewhat different from melting of Cu-Ni bimetallic clusters (Balbuena, P.B and Huang, S.P, 2002), where outward movement of Ni was countered by the inward movement of Cu maintaining an overall spherical shape. This difference in behavior is explained below on the basis of relative surface energy change with temperature for the two bimetallics.

4.2.3 Concept of Surface Energy

Table 4 shows the surface energy difference at 0 K for a Pd-Pt system, when entropic factors are zero. The typical surface energy differences are between 15-45 KJ/mol depending on the coordination numbers (Mezey, 1982). The mixing energy values for Pd and Pt are -8.44 and 7.24 KJ/mol. The cluster microstructure at any temperature depends on the interplay among these three factors. At low temperatures, we find the segregation dependent primarily on the surface energy difference. For an ideal bimetallic alloy, with 50% composition, the entropy of mixing increases from 2 KJ/mol at 298 K to 7.4 KJ/mol near the melting point (1290 K for $(Pd_{0.5}\text{-}Pt_{0.5})_{456}$ cluster). The surface energy difference between the two, however, increases with increasing temperature as shown in Figure 5.

Table 4. Surface energy of Pd and Pt at various coordination sites

Coordination Number	γ_{Pd} (KJ/mol)	γ_{Pt} (KJ/mol)
6 (corner)	175.6	218.1
7(edge)	145.7	178.5
8(fcc(100))	115.8	139.9
9(fcc(111))	85.9	100.3

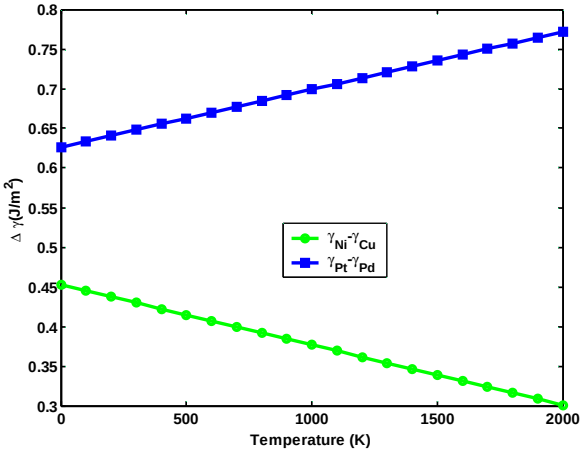

Figure 5. Variation of surface energy difference with temperature for Pd-Pt (blue line with rectangles) and Cu-Ni (green line with circles) systems

The surface energies of both Pd and Pt decrease with temperature. Hence both Pd and Pt atoms would tend to locate themselves at the surface. However, an increase in the surface energy difference would mean that the decrease in surface energy of Pd atoms is much more than that of Pt. Hence Pd would continue to remain at the surface. Also, owing to the decrease in the absolute surface energy, Pt too prefers to move to the surface. The combined effect results in a net movement of atoms to the surface. This is clearly evident from the deformation parameter plot where ε_r^{Pt} increases sharply indicating the outward movement of Pt atoms. On the other hand, ε_r^{Pd} remains almost constant suggesting little movement of Pd atoms to the core. This behavior is different from a Cu-Ni bimetallic where the surface energy difference decreases with an increase in temperature showing that the decrease in surface energy of Ni overcomes that of Cu, resulting in migration of Ni atoms to the outside and that of Cu atoms to the inside.

4.2.4 Surface Melting and Lindemann Criterion

Surface melting refers to the formation and propagation of a quasi-liquid film, which thickens with increasing temperature and ends with the melting of the solid core. The temperature at which the film thickness diverges to infinity corresponds to the bulk melting point.

Insights into this phenomenon could be obtained by partitioning the cluster into five radial shells of equal width dR and calculating the mean square displacement in each shell to estimate the self diffusion coefficients (Haile, 1992) for atoms in that shell using Eqn. (4.4)

$$D \equiv \frac{1}{2d} \lim_{t \to \infty} \frac{\left\langle [r(t_0 + t) - r(t_0)]^2 \right\rangle}{t} \qquad (4.4)$$

The inter-atomic distance between atoms in the Pd-Pt bimetallic (2.75 A) was used as dR and the atoms were assigned to the bins based on their initial positions at the end of the equilibration period. The mean square displacements for each shell were then generated by averaging over a 25 ps trajectory with sampling done every 0.1 ps. Averages taken over 25ps trajectory with different origins gave the same result which is indicative of a system that is truly in equilibrium.

Figure 6 shows that the diffusivities of outer shells are higher than the inner ones. In accordance with the Lindemann criterion, which predicts the occurrence of phase transition when atomic motions exceed 10-15% of inter-atomic distance (2.75 A), there exists a critical diffusivity (3e-10 m^2/s) indicating transformation to a liquid phase.

Based on this, we find that in the temperature range 900-1100, only the fifth bin is molten. As temperature increases (1200 K), atoms in the fourth and fifth bins reach the critical value, while those in the first three remain crystalline. At the melting point (1290 K), the diffusivity of the entire cluster exceeds the critical value. We can estimate the $R_{crystal}$ or the solid core remaining based on the shell diffusivity plot.

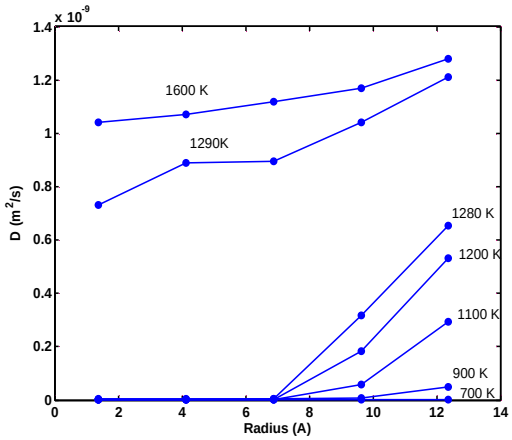

Figure 6. Diffusion coefficients calculated for atoms in various shells for $(Pd_{0.5}\text{-}Pt_{0.5})_{456}$ as a function of distance from the center of cluster

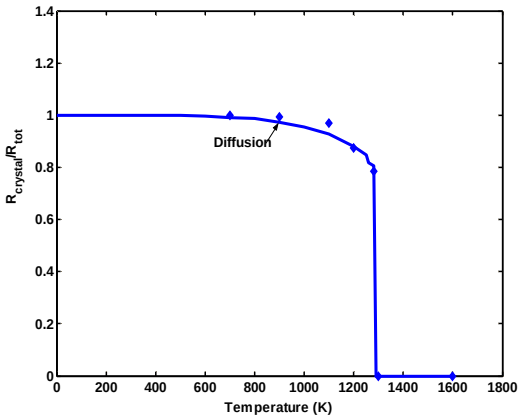

Figure 7. Radius of solid core in $(Pd_{0.5}\text{-}Pt_{0.5})_{456}$ cluster as a function of temperature during the melting process calculated from two procedures: The diamonds indicate values obtained by assuming a critical diffusivity of 3e-10 (m2/s) similar to Lindemann criterion. The line is based on crystal radius obtained by calculated deviations from linearity in the potential energy curve (Figure 1).

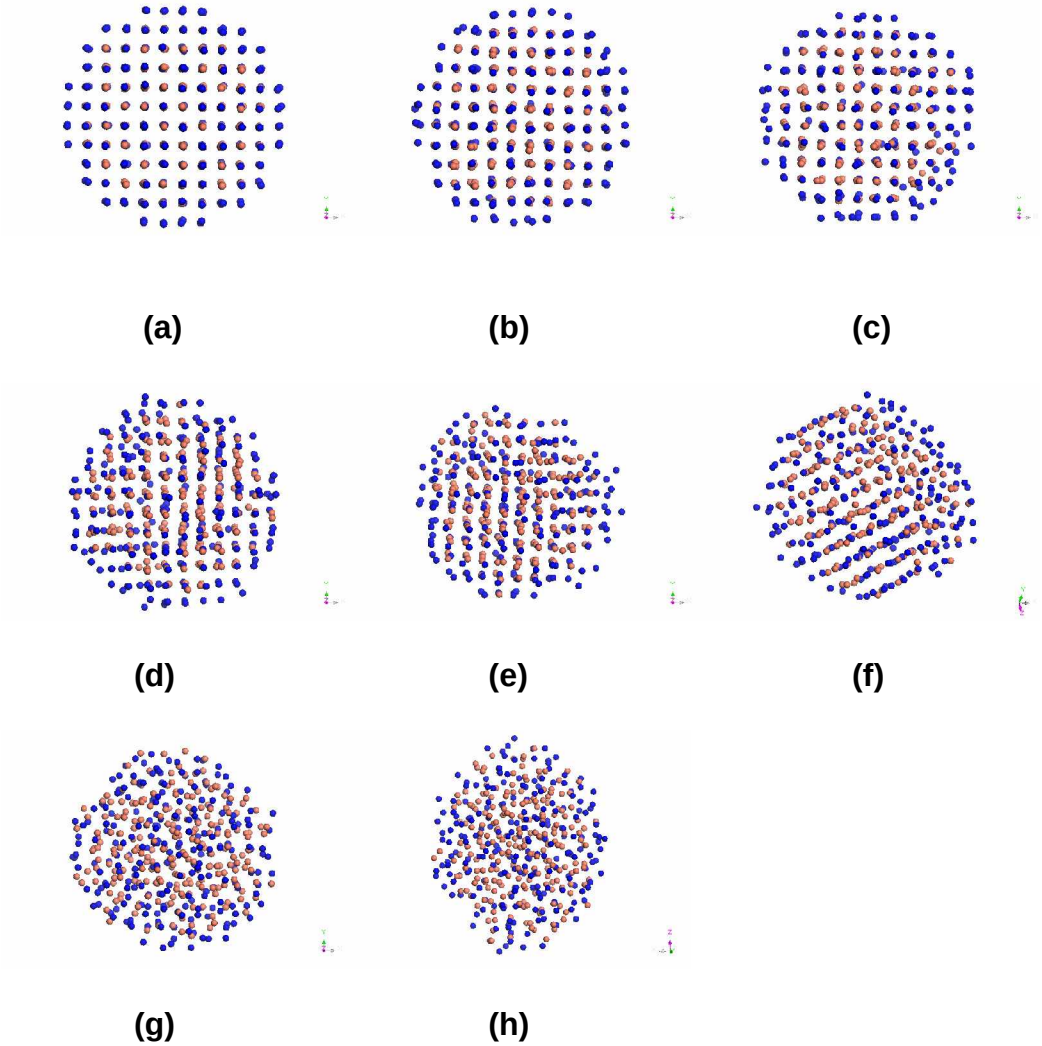

Figure 8. Snapshots of $(Pd_{0.5}\text{-}Pt_{0.5})_{456}$ cluster taken at various temperatures indicating surface melting of Pd followed by homogeneous melting of Pt core. (a) 300 K (b) 700 K (c) 900 K (d) 1100 K (e) 1200 K (f) 1280 K (g) 1290 K (h) 1800 K

$R_{crystal}$ can also be estimated from the heat of fusion (Qi et al, 2001). The deviation from linearity in the potential energy curve (ΔPE) gives an extent of surface melting (Figure 1). Radius of the solid core remaining at any point during the melting process (Figure 7) can be given by

$$\frac{R_{crystal}}{R_{total}} = \left(1 - \frac{\Delta PE}{L}\right)^{1/3} \tag{4.5}$$

The surface melting phenomenon is clearly evident from the snapshots taken at various temperatures (Figure 1). The change in shape of the cluster is also observed.

4.2.5 Shape transformation during melting

Moment of inertia tensor can be used to characterize the shape transformation associated with melting. The moment of inertia (MI) is a second rank tensor and has nine components as given in Eqn. (4.6),

$$I_{jk} = \int_V \rho(r)(r^2\delta_{jk} - x_j x_k)dV \tag{4.6}$$

These can be used to gain insights into the changes in cluster shape. The tensor components calculated at different temperatures are summarized in Table 5. In all the calculations, the mass of Pd and Pt has been assumed to be same. The change in MI is then dependent only on the relative distance of the atoms from the cluster centre of mass.

Table 5. Tensor components of moment of inertia at different temperatures

Temp. (K)	Ixx (A^2)	Iyy (A^2)	Izz (A^2)	-Ixy=-Iyx (A^2)	-Iyz=-Izy (A^2)	-Izx=-Ixz (A^2)
300	24964.53	24934.33	24957.08	-46.01	-55.21	41.82
900	25136.82	25774.93	26054.08	64.24	-192.62	-199.69
1280	25803.87	27379.53	25844.87	272.52	264.25	1338.07
1290	26281.85	27312.61	27304.85	-485.17	-1166.93	611.13
1800	28488.78	28606.83	26983.60	-752.83	1861.21	-1505.03

As shown in Table 5 , the cluster structure initially is spherical with diagonal elements $I_{xx}=I_{yy}=I_{zz}$ and the off diagonal elements having much lower values. MI increases with temperature indicating that the atoms have a tendency to move away from the centre of mass. Near the melting point (1290K), the cluster has a shape closer to that of an ellipsoid ($I_{xx}=I_{zz}$) with the off-diagonal elements having higher values than before. At higher temperatures after phase transition occurs, the cluster remains more or less an ellipsoidal shape ($I_{xx}=I_{yy}$). The same is indicated by principal moment of inertia as shown in Table 6 and the snapshots in Figure 8.

Table 6. Principal components of moment of inertia at different temperatures

Temp.(K)	$I_1 \times 10^4$ (A^2)	$I_2 \times 10^4$ (A^2)	$I_3 \times 10^4$ (A^2)
300	2.4854	2.4998	2.5004
1280	2.4455	2.7183	2.7428
1290	2.5432	2.6988	2.8478
1800	2.4969	2.9231	2.9879

4.3 Effect of Composition on Melting

The melting characteristics were investigated for different compositions of the bimetallic, namely, 5%, 25%, 75% and 95% Pt using the potential energy variation and the result

summarized in Table 7. The melting point increases progressively with the Pt concentration in the bimetallic as shown in Figure 9.

The melting point could be related to the composition for 456 atom cluster by,

$T_m = 3.4X + 1100$

where X is the percentage composition of Pt.

This nearly linear behavior is seen even for larger cluster sizes (1088 atoms) as shown in Figure 9. In calculating the melting points for different compositions, we used the jump in potential energy corresponding to the melting of the Pt rich cluster core. The linear variation of melting point can be attributed to the proportional change in the radius of the solid Pt core with composition. In addition, we find that clusters which are rich in Pd show surface melting to a greater extent. This feature is characterized by increasing deviations of the potential energy curve from linearity with increasing Pd composition.

Table 7. Variation of melting point with composition for the 456 and 1088 atom clusters respectively

Composition	Melting point (K)	
	1088 atoms	456 atoms
5% Pt	1250±10	1120±10
25%Pt	1340±10	1200±10
50%Pt	1460±10	1280±10
75%Pt	1540±10	1370±10
95%Pt	1600±10	1430±10

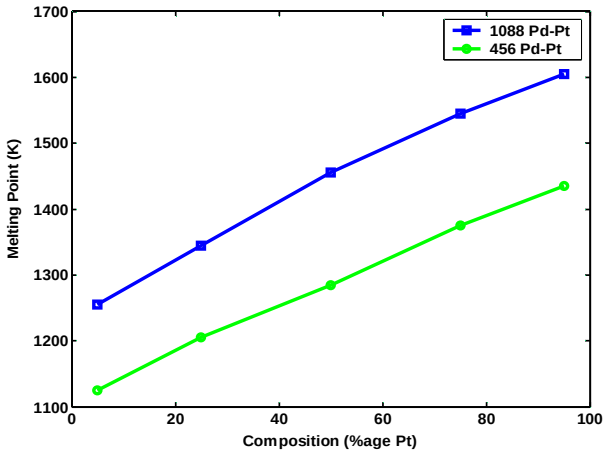

Figure 9. Melting point variations with composition for $(Pd_{0.5}\text{-}Pt_{0.5})_{456}$ (green line with circles) and $(Pd_{0.5}\text{-}Pt_{0.5})_{1088}$ (blue line with rectangles)

Metal nanoclusters used to carry out chemical reactions at high turnover and selectivity often operate in 400-1000 K range (Zhou, 2004). In sensor applications, the gas adsorption mechanism is primarily dependent on the surface morphology. DFT studies as well as experiments indicate certain sites such as Pd (111) are more preferred for O_2 adsorption than Pd (110) (Hansen, 2002). The selectivity, sensitivity and the speed of response is then influenced by the relative densities of such sites. As temperature increases, the movement of surface atoms as a result of surface melting can have an important effect on the catalytic and sensing activity. Understanding the variation of surface melting characteristics with compositions could help optimize the operating conditions required for catalysis and sensing.

4.4 Bulk melting of Pd and Pt.

To justify the choice of the QSC potential with the listed parameters used in the MD simulations, bulk melting of Pd and Pt was carried out using the same models with periodic boundary conditions in a constant NPT system and the results are summarized in Table 8. The calculated melting points from the simulations agree well with the bulk experimental values of Pd and Pt. The slight differences could be attributed to the empirical nature of the potential function. The enthalpy of melting also compares well with the experimental values.

Table 8. Comparison of bulk simulation results with experimental values.

	Melting Point of Pd (K)	Melting Point of Pt (K)	ΔH(Pd) KJ/mol	ΔH(Pt) KJ/mol
Experiments	1840	2040	16.7	20
Bulk Simulation	1760	2090	15.8	18.74

5 Conclusions

The melting behavior of Pd-Pt nanoclusters having 456 and 1088 atoms is characterized by pre-melting of surface segregated Pd atoms followed by homogeneous melting of Pt core. The melting point of the nanoclusters is clearly identified by studying the variation in potential energy and specific heat capacity. The melting point of nanoclusters calculated from our simulations is much lower than the corresponding bulk Pd and Pt crystals. The bond order parameters indicate a change from an FCC type structure to an HCP one before transformation to a liquid phase. As melting proceeds, the Pd atoms tend to diffuse inside while the Pt atoms diffuse outside. The extent of diffusion is not the same, leading to a net increase in the number of surface atoms characterized by shape change from spherical to somewhat oval. This melting behavior is different from some of the bimetallics (for example, Cu-Ni) studied earlier. The difference in behavior can be explained on the basis of variation of surface energy difference with temperature. The surface melting phenomenon is indicated by the deviation of potential energy curve from linearity. Shell based self diffusion coefficients give better insights into the surface melting phenomenon. The melting phenomenon was studied for different compositions and a linear trend was observed for both 456 and 1088 atom cluster.

The description of the melting transition agrees qualitatively with previous simulation and experimental studies on nanoclusters.

Acknowledgements

Partial support was provided by NASA-Glenn via FSEC, Florida. The Daresbury Laboratory provided the DL_POLY package. The authors also want to thank Ling Miao and Reetu Singh for some valuable discussions. Evaluation version of DMOL3 package was used in generating Figure 8 in this paper.

References

1) Allen, M.P and Tildesley, D.J. Computer Simulation of Liquids, 1987, Oxford University Press.
2) Baletto, F.; Mottet, C.; Ferrando, R. Phys. Rev. Lett. 2003, 90(13), 135504-1-135504-4.
3) Berendsen, H. J. C.; Postma, J. P. M.; Van Gunsteren, W. F.; DiNola, A.; Haak, J. R. J. Chem. Phys. 1984, 81(8), 3684-3690.
4) Bromley, S. T.; Sankar, G.; Catlow, C.R.A.; Thomas, J. M.; Maschmeyer, T. Micropor. Mesopor. Mater. 2001, 44-45, 395-399.
5) Buffat, Ph. and Borel, J-P. Phys. Rev. A 1976, 13(6), 2287-2298.
6) Cagin, T.; Kimura, Y.; Qi, Y.; Li, H.; Ikeda, H.; Johnson, W.L.; Goddard, W.A. III. Mater. Res. Soc. Symp. Proc. 1999, 554(Bulk Metallic Glasses), 43-48.
7) Calvo, F. and Spiegelmann, F. J. Chem. Phys. 2000, 112(6), 2888-2908.
8) Chaudhari, A. 2004, Master's Thesis (USF).
9) Chushak, Y.G. and Bartell, L.S. J. Phys. Chem. B 2003, 107(16), 3747-3751.
10) Chushak, Y.G.; Bartell, L.S. J. Phys. Chem. B 2001, 105(47), 11605-11614.
11) Cleveland, C.L.; Luedtke, W.D.; Landman, U. Phys. Rev. Lett. 1998, 81(10), 2036-2039.
12) Favier F, Walter EC, Zach MP, et al. Science 2001, 293 (5538): 2227-2231.
13) Foiles, S.M.; Baskes, M.I., and Daw, M.S. Phys. Rev. B 1986, 33, 7983.
14) Haile, J. M., Molecular Dynamics Simulations: Elementary Methods (John Wiley and Sons. New York, 1992).
15) Hansen, K.H; Sljivancanin, Z.; Laegsgaard, E.; Besenbacher, F.; Stensgaard, I. Surf. Sci. (2002), 505(1-3), 25-38
16) Huang, S.P. and Balbuena, P.B. J. Phys. Chem. B 2002, 106(29), 7225-7236.
17) Jin, Z. H.; Sheng, H. W.; Lu, K. Phys. Rev. B 1999, 60(1), 141-149.
18) Kusche, R.; Hippler, Th.; Schmidt, M.; Von Issendorff, B.; Haberland, H. Eur. Phys. J. D 1999, 9(1-4), 1-4.
19) Lee, Y.J.; Lee, E.K.; Kim S.; Nieminen R.M. Phys. Rev. Lett. 2001, 86(6), 999-1002.
20) Lei, H. J. Physics 2001, 13(13), 3023-3030.
21) Lewis, L.J.; Jensen, P.; Barrat, J.L. Phys. Review B 1997, 56(4), 2248-2257.
22) Lopez, M. J.; Marcos, P. A.; Alonso, J. A. J. Chem. Phys. 1996, 104(3), 1056-66.
23) Mainardi, D.S. and Balbuena, P.B. Langmuir 2001, 17, 2047-2050.
24) Mezey, L.Z. and Giber, J. Jpn. J. Appl. Phys., Part 1, 1982, 21(11), 1569-1571.
25) Morishita, T. J. Chem. Phys. 2000, 113(8), 2976-2982.
26) Ozdemir, K. S.; Tomak, M.; Uludogan, M.; Cagin, T. J. Non-Cryst. Solids 2004, 337(2), 101-108.
27) Petroski, J.M.; Wang, Z.L.; Green, T.S; El-Sayed, M.A. J. Phys. Chem. B 1998, 102(18), 3316-3320.
28) Qi, Y.; Cagin, T.; Johnson, W.L.; Goddard, W.A. III. J. Chem. Phys. 2001, 115(1), 385-394.
29) Qi, Y.; Cagin, T.; Kimura, Y.; Goddard, W.A. III. Phys. Rev. B 1999, 59(5), 3527-3533.
30) Qi, Y.; Cagin, T.; Kimura, Y.; Goddard, W.A. J. Comput. Aided Mater. Des. 2001, 8(2-3), 233-244.
31) Qi, Y.; Cagin, T.; Kimura, Y.; Goddard, W.A.III. Phys. Rev. B 1999, 59(5), 3527-3533.
32) Rafii-Tabar, H. and Sutton, A. P. Philos. Mag. Lett. 1991, 63(4), 217-224.

33) Schmidt, M.; Kusche, R.; Kronmuller, W.; Von Issendorff, B.; Haberland, H. Phys. Rev. Lett., 1997, 79(1), 99-102.
34) Shvartsburg, A.A. and Jarrold, M.F. Phys. Rev. Lett. 2000, 85(12), 2530-2532.
35) Sinfelt, J. H. Bimetallic Catalysts-Discoveries, Concepts, and Applications, 1983, John Wiley & Sons, New York.
36) Steinhardt, P.J.; Nelson, D.R.; Ronchetti, M. Phys. Rev. B 1983, 28(2), 784-805.
37) Strohl, J.K. and King, T.S. J. Catalysis 1989, 118(1), 53-67.
38) Strohl, J.K.; King, T.S. J. Catalysis 1989, 116(2), 540-555.
39) Sutton, A. P and Chen, J. Philos. Mag. Lett. 1990, 61, 139-146.
40) Walter E. Metal Clusters. 1999, Wiley series in theoretical chemistry.
41) Wang, J.; Ding, F.; Shen, W.; Li, T.; Wang, G.; Zhao, J. Solid State Comm. 2001, 119(1), 13-18.
42) Wang, Z.L; Petroski, J.M.; Green, T.C.; El-Sayed, M.A. J. Phys. Chem. B 1998, 102(32), 6145-6151.
43) Yang, L. and DePristo, A.E. J. Catalysis 1994, 148(2), 575-586.
44) Yang, L. and DePristo, A.E. J. Catalysis 1994, 149(1), 223-228.
45) Zhou, B.; Hermans, S.; Somarjai, G.A. Nanotechnology in Catalysis, Vol. 1 and 2, 2004, Kluwer Academic/Plenum Publishers, New York.
46) Zhu, L. and DePristo, A.E. J. Catalysis 1997, 167(2), 400-407.
47) Zhu, L. and DePristo, A.E. J. Chem. Phys. 1995, 102(13), 5342-5349.
48) Zhu, L. and DePristo, A.E. J. Chem. Phys. 1995, 102(13), 5342-5349.
49) Zhu, L.; Wang, R.; King, T.S.; DePristo, A.E. J. Catalysis 1997, 167(2), 408-411.